Advances in Computational Design, *Vol. 1, No. 4 (2016) 357-370*
DOI: http://dx.doi.org/10.12989/acd.2016.1.4.357

Shock analysis of a new ultrasonic motor subjected to half-sine acceleration pulses

Xiaoyan Hou*, Heow Pueh Lee, Chong Jin Ong and Siak Piang Lim

Department of Mechanical Engineering, National University of Singapore, 21 Lower Kent Ridge Road, Singapore

(Received July 27, 2016, Revised September 2, 2016, Accepted October 4, 2016)

Abstract. This paper aims to examine the dynamic response of a newly designed ultrasonic motor under half-sine shock impulses. Impact shock was applied to the motor along x, y or z axis respectively with different pulse widths to check the sensitivity of the motor to the shocks in different directions. Finite Element Analysis (FEA) with the ANSYS software was conducted to obtain the relative displacement of a key point of the motor. Numerical results show that the maximum relative displacement is of micro meter level and the maximum stress is five orders smaller than the Young's modulus of the piezo material, which proves the robustness of the motor.

Keywords: standing wave ultrasonic motor; shock analysis; finite element method; piezoelectric stack

1. Introduction

Ultrasonic motors are powerful and precision-controlled actuators developed over the past four decades (Vasiljev 2008, Sashida and Kenjo 1993). In an ultrasonic motor, a voltage is applied to the piezoelectric ceramic element(s). Due to the converse piezoelectric effect, alternating oscillations in the ultrasonic range are generated at the driving head of the motor, which then drives a rotor/slider to perform unidirectional movement (Guo *et al*. 2012). Though the magnitude of a cycle of the movement is small (of the order of micrometers), high speed motion (of the order of millimeters to centimeters per second) is possible using high frequency driving signals (Paik 2009, Busch-Vishniac 1999).

Ultrasonic motors have several unique advantages. They are neither affected by nor create magnetic field and are quiet since ultrasonic vibrations are inaudible to humans (Yang 2016, Zhao 2007). Ultrasonic motors are also considered superior in the mini-motor area as their efficiency is insensitive to size (Uchino 1999). As piezoelectric elements are used as functioning elements, ultrasonic motors are characterized by quick response and precision controllability (Sashida and Kenjo 1993, Ikeda 1990, Randeraat and Setterington 1974). These merits have attracted industrial and research interests and led to the development of many ultrasonic motors.

As ultrasonic motors have a short history, new or novel ultrasonic motor designs are desirable

*Corresponding author, Research Fellow, E-mail: houxiaoyan@gmail.com

http://www.techno-press.com/journals/acd&subpage=7 ISSN: 2383-8477 (Print), 2466-0523 (Online)

for various potential applications. Recently, a new standing wave ultrasonic motor was proposed by the authors (Xiaoyan *et al*. 2012). It is a general purpose ultrasonic motor featured with three piezoelectric stacks connected to a central block. The motor has a quick response and reaches steady state within 1.5 ms. High-speed positioning of decimal meter per second can be achieved to implement rapid moving tasks. Due to the specific design of the motor, the movement in two translations can be controlled independently and the speed can be changed by adjusting the amplitude of the voltage. The motor also self-locks after the power is off and has a quiet operation.

Shock analysis is important for various precision devices to understand their dynamic behavior under impacts. For example, a thorough understanding of the actuator arm response under a drop is essential to improve the reliability of a new model of Hard Disc Drive (Shu *et al*. 2007, Chan and Liao 2008). Finite Element Method is frequently utilized in shock analysis to reduce the expensive and time-consuming process of prototype testing.

For the motor proposed by Xiaoyan *et al*. in 2012, besides the characteristics such as high speed positioning, it must be robust too to resist shock. This paper aims to numerically examine the dynamic response of the motor under half-sine shock impulses. The relationship between the response of the motor and its mode shapes will also be addressed.

2. Structure of the motor

The newly designed ultrasonic motor contains three piezoelectric stacks and one aluminum central block, as shown in Fig. 1. The upper and lower PZT stacks are symmetrical in both geometric and material characteristics. The right PZT stack is made of the same PZT material but its dimensions may be different. All the three stacks have one end connected to the central block and the other end clamped to an enclosure case.

The piezoelectric stacks are essential actuating components of the motor. In the proposed motor, PZT from Fuji Ceramics C-6 series are employed due to their high piezoelectric charge constants and mechanical quality factor. Table 1 lists the important material and geometric properties of a prototype motor. The polarization direction and the orientation of the electric field applied to the blocks are both along the stack length direction, normal to the electrode surfaces.

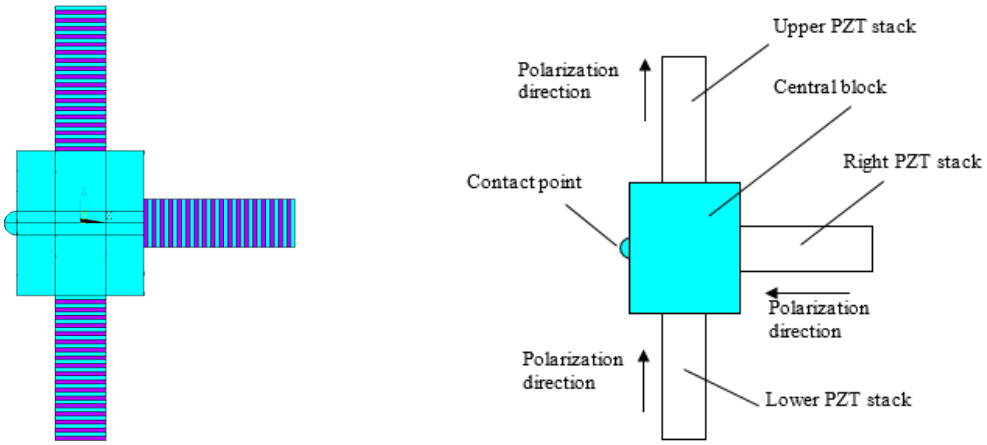

Fig. 1 Schematic of the proposed motor

Table 1 Material and geometric properties of the prototype motor

	Unit	Nomenclature	
Density	kg/m^3	ρ	7400
Poisson's Ratio		σ^E	0.31
Elastic Modulus (e Formal)	×10^{10} N/m^2	C_{11}^E	12.3
		C_{12}^E	7.7
		C_{13}^E	8.0
		C_{33}^E	11.2
		C_{44}^E	1.9
		C_{66}^E	2.3
Piezoelectric Charge Constants	×10^{-12} m/V	d_{31}	-210
		d_{33}	472
		d_{15}	758
Relative Dielectric Constants		$\varepsilon_{11}^S / \varepsilon_0$	1039
		$\varepsilon_{33}^S / \varepsilon_0$	749
Coupling Factors	×10^{-2}	K_{31}	40.9
Mechanical Q		Q_m	110
Upper & lower stack dimensions	mm		12×3×4
Right stack dimensions	mm		12×4.6×4
Central block dimensions	mm		12×10×4

The motor is clamped into an enclosure case via the "fixed" ends of the PZT stacks. During shock, the energy of the shock impulse is transferred from the enclosure case to the motor through the "fixed" ends of the stacks. When the motor is dropped onto a surface, it experiences a reaction acceleration pulse from the surface. The shock received by the motor in terms of both amplitude and pulse width is affected by the contact surface stiffness and the drop height (Brian W Lang 10). The harder the ground surface, the magnitude will be larger and the duration of the pulse will be shorter.

3. Finite element analysis

Finite Element Analysis (FEA) is used in this study to obtain the dynamic response of the motor under shock with ANSYS software. The FEM model of the prototype motor is presented in Fig. 2. It consists of two main parts: elastic parts and piezoelectric parts. The elastic parts are modeled by SOLID73, a 3D solid element defined by eight nodes. Each node has six Degrees of Freedom (DOFs): translations in the nodal *x*, *y* and *z* directions and rotations about the nodal *x*, *y* and *z* axes. The piezoelectric blocks are modeled by SOLID5, a 3D coupled-field solid finite

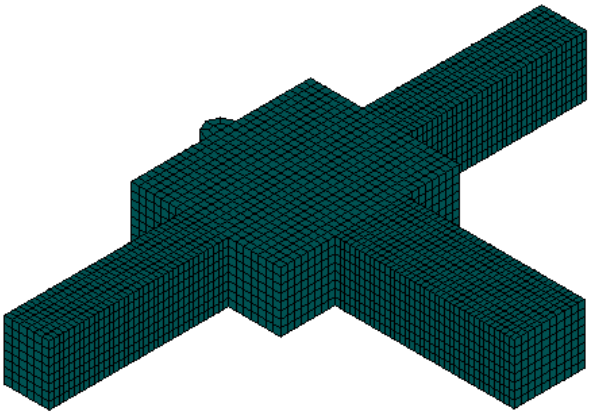

Fig. 2 FEM model of the prototype motor

element. SOLID5 element has eight nodes and each node has up to six DOFs plus electrical potential (voltage). The connecting layers between the PZTs and the aluminum block are so thin with respect to the PZTs that their mechanical effect is neglected in the following numerical analysis.

Hexahedral (brick) volume elements are utilized to generate the mapped mesh as shown in Fig. 2. The mesh size is set to be 0.5 mm and the three dimensional model has a total of 10576 elements. To check the appropriateness of the mesh density, the element size was decreased from 0.5 mm to 0.4 mm to refine the mesh. Consequently, the element number increased to 20143, which was about double of the previous element number. By redoing analyses using the refined model, it was found that the two meshes gave nearly the same results. For instance, the difference in the natural frequencies obtained from the two meshed models was within 0.05%. This means that the selected mesh size of 0.5 mm is adequate. During solution process, the convergence norms were calculated and compared with the corresponding convergence criteria. It was found that the convergence norms were about 10% of the criteria and the solution converged after one or two iterations.

For shock analysis, the motor is fixed into an external case via the three “fixed” ends of the stacks. The boundary condition of the model is that the DOFs of all the nodes on the “fixed” ends are fully constrained except the translational DOFs in the drop direction. In addition, all the DOFs of the nodes at the “fixed” ends are coupled together in the drop direction to simulate that these nodes experience the same shock. For each PZT layer in the stacks, two of its opposite surfaces are covered by electrodes, resulting in equal potential surfaces. To simulate this terminal condition in ANSYS, all voltage DOFs of the nodes on the positive or negative electrode surface are coupled together to have the same electrical potential and/or current.

In the following, modal analysis will be first carried out to obtain the mode shapes and natural frequencies of the ultrasonic motor. Transient analysis will then be implemented to investigate the dynamic response of the motor under half-sine impulse shock. The pulse width effect on the motor response will also be examined to check the robustness of the ultrasonic motor.

3.1 Modal analysis

When a half-sine shock along *z* axis is applied to the motor, the translational u*x* and u*y* and the rotational rot*x*, rot*y* and rot*z* are constrained at the "fixed" ends of the motor. Only the translational u*z* of the nodes on the "fixed" ends are not constrained (Fig. 3). On the contrary, they are coupled together to have the same input impulse and output motion. Through modal analysis, the natural frequencies and mode shapes of the ultrasonic motor can be determined (Fig. 4). Modal analysis is necessary in understanding the inherent properties of the motor. They will also be compared with the transient analysis results which will be obtained in the following sub-section.

For drop direction along *x* or *y* axis, modal analysis was also conducted. The difference in the boundary condition is the DOFs to be coupled together. For instance, when the drop is applied along *x* axis, the DOF of u*x* at the "fixed" ends of the PZT stacks are coupled together. It was found that for different drop direction, the modal frequencies and mode shapes were almost the same with a slight difference within 0.01%.

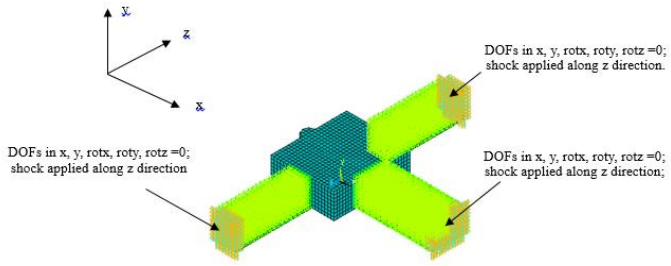

Fig. 3 FEM model of the motor under a shock along *z* axis

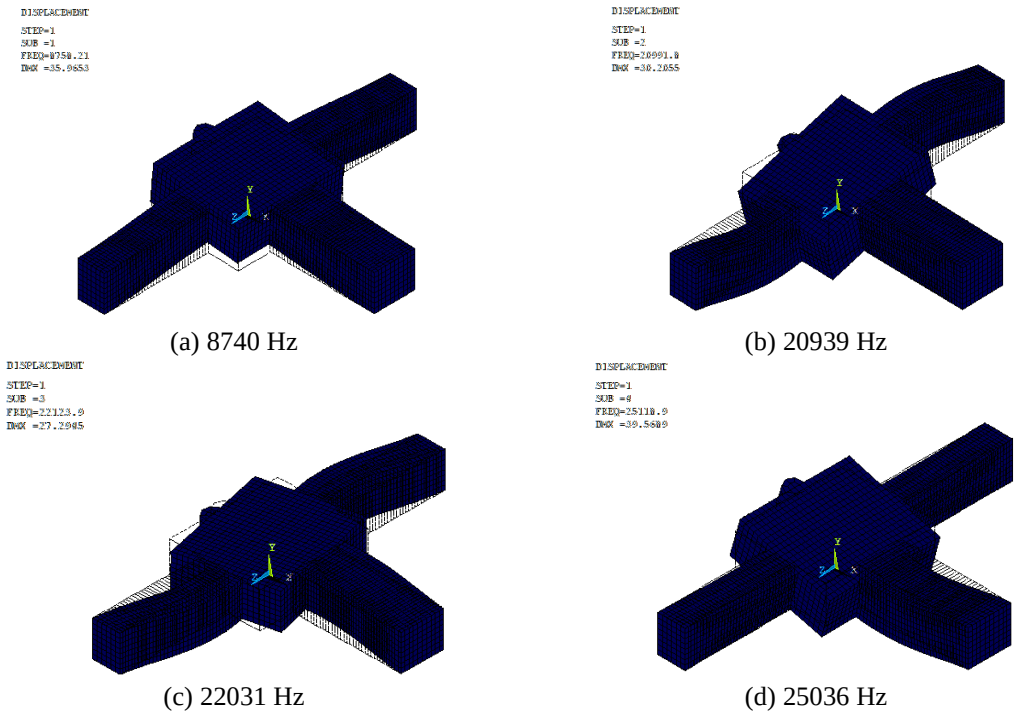

(a) 8740 Hz (b) 20939 Hz

(c) 22031 Hz (d) 25036 Hz

Fig. 4 The first eight mode shapes of the motor

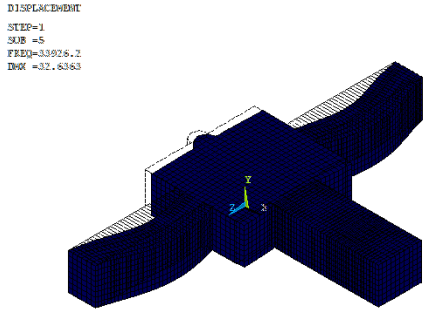

(e) 33587 Hz

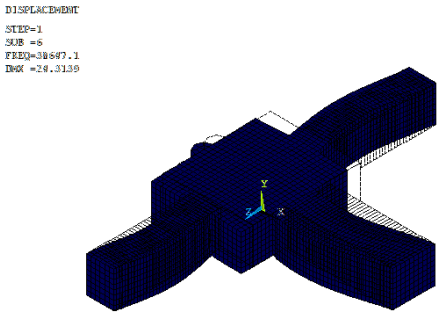

(f) 38113 Hz

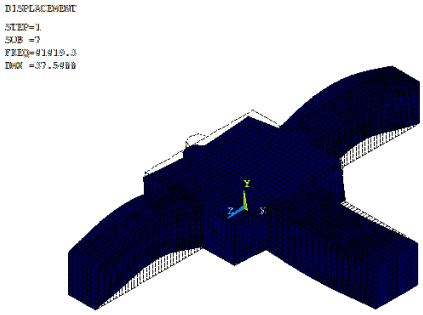

(g) 41158 Hz

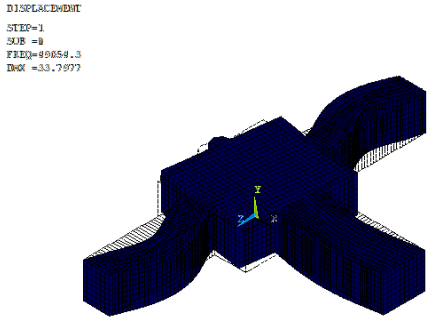

(h) 48421 Hz

Fig. 4 Continued

3.2 Transient analysis

Transient dynamic analysis, sometimes known as time-history analysis, is a technique used to determine the dynamic response of a structure under the action of any general time dependent loads. This type of analysis is used to determine the time-varying displacements, stresses, strains and forces as it responds to any combination of static, transient and harmonic loads (ANSYS, 2010). In this paper, transient analysis is carried out to examine the response of the motor to different shock loadings.

In order to evaluate the response of the motor to different impact conditions, a series of transient simulations were carried out. The shock was applied to the motor along z, x or y axis respectively to check the sensitivity of the motor to the shocks in different directions. In each shock direction (for instance, along z axis), the motor was under a 600 g (g is the gravitational acceleration) half-sine acceleration shock. The acceleration level of 600 g is close to the design shock limit of portable devices like Hard Disc Drives (HDDs). The pulse duration for each simulation ranges from 2 ms, 0.5 ms to 0.125 ms. The duration of 0.125 ms could correspond to a hard surface like a concrete pavement and 2 ms could represent a softer surface like a carpeted floor. Fig. 5 shows the three shock pulses used in the following shock simulations. They are applied to the motor one by one along each shock direction.

The half-sine profile in Fig. 5 is an acceleration function. In ANSYS, it is difficult to be directly applied to the nodes on the "fixed" ends of the stacks. Therefore the acceleration function was integrated twice to obtain the displacement function as the equivalent shock input into ANSYS as shown below:

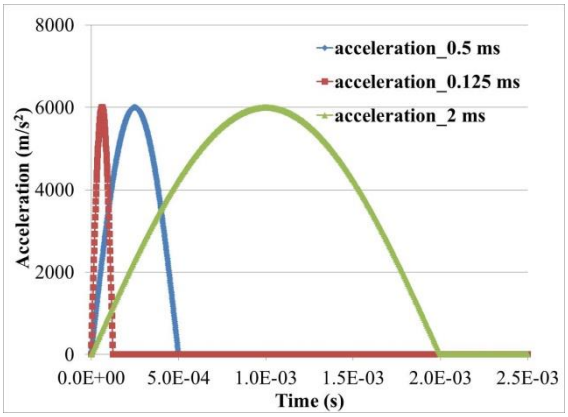

Fig. 5 Acceleration profile of the 600 g applied to the motor for a pulse width of 0.125 ms, 0.5 ms and 2 ms

The half-sine acceleration can be described as

$$\ddot{Z} = \begin{cases} A\sin(2\pi ft) & t \le T \\ 0 & t \ge T \end{cases}$$

where A is the magnitude of the shock, t is the time variable and T is the pulse width.

Integrating from acceleration to velocity at the ends of the stacks, we have

$$\dot{Z} = \begin{cases} -\dfrac{A}{2\pi f}\cdot\cos(2\pi ft) + \dfrac{A}{2\pi f} & t \le T \\ \dfrac{A}{\pi f} & t \ge T \end{cases}$$

The velocity is integrated again to obtain the displacement

$$Z = \begin{cases} -\dfrac{A}{4\pi^2 f^2}\cdot\sin(2\pi ft) + \dfrac{A}{2\pi f}\cdot t & t \le T \\ \dfrac{A}{\pi f}\cdot t - \dfrac{A}{4\pi f^2} & t \ge T \end{cases}$$

At $t=T$, the displacement Z and the velocity $\dot{Z}$ are $\dot{Z} = \dfrac{A}{\pi f}$ and $\dot{Z} = \dfrac{A}{4\pi f^2}$ respectively.

As the motor is a light damping device, the structural damping in the simulations was set to be 1% as an illustration. Cases with other damping ratio (e.g., 0.2%, 0.5% and 2%) were also investigated. It was found that the different damping ratio results in only slight difference in displacement magnitude. A Full Transient Dynamic Analysis was used in the calculation. This leads to more accurate results compared to those obtained by the Reduced or Modal Superposition methods (Zeng and Bogy 2002). However this calculation method takes much longer time and more computational resource.

The relative displacement of the contact point as illustrated in Fig. 1 is an important parameter for motor design as the motor periodically contacts the rotor at this point during its normal operation. It is desired to be small so that the motor and rotor do not badly impact with each other when the motor experiences a shock. The relative displacement is defined as the displacement of the contact point minus the displacement of the right "fixed" end.

For different shock input in Fig. 5, the response of the contact point was obtained via transient analysis. Using the impulse width of 0.5 ms as an illustration, as shown in Fig. 6(a), the amplitude of the displacements in all the three translational directions gradually decreases with time. The maximal relative displacement is 6.72×10^{-8} meter occurring at 0.53 ms. Due to the symmetric structure of the motor in *xz* plane, upon the impulse applied along OZ direction, the relative displacement at the contact point is thousands of times larger than u*y* and u*x*. The calculation time for one transient analysis is about 6 hours.

From Fig. 6, it is also observed that for the time period within the pulse width, the relative displacement may be fitted by a half-sine curve, which has the same period as the input acceleration pulse. For the oscillations after the pulse width (e.g., 0.5 ms ~ 1.0 ms), it is the superposition of sine waves with different periods, reflecting the higher vibration modes excited by the impulse. For instance, one of the peak to peak periods is 0.021 ms, which corresponds to 47059 Hz. From modal analysis, it reflects the 8th vibration mode of the motor, whose natural frequency is 48421 Hz (Fig. 4(h)). The discrepancy in the frequencies is due to the time step resolution of 0.00125 ms. 47059 Hz is the closest value to the frequency of 48421 Hz.

The oscillations have the same period of 0.045 ms which corresponds to a frequency of 22038 Hz. This frequency is quite near the modal frequency of 22031 Hz of the motor (Fig. 4 (c)). In this mode, the three beams undergo their 1st order bending in the *xz* plane. The natural frequencies obtained from the modal and the transient analyses almost coincide with each other.

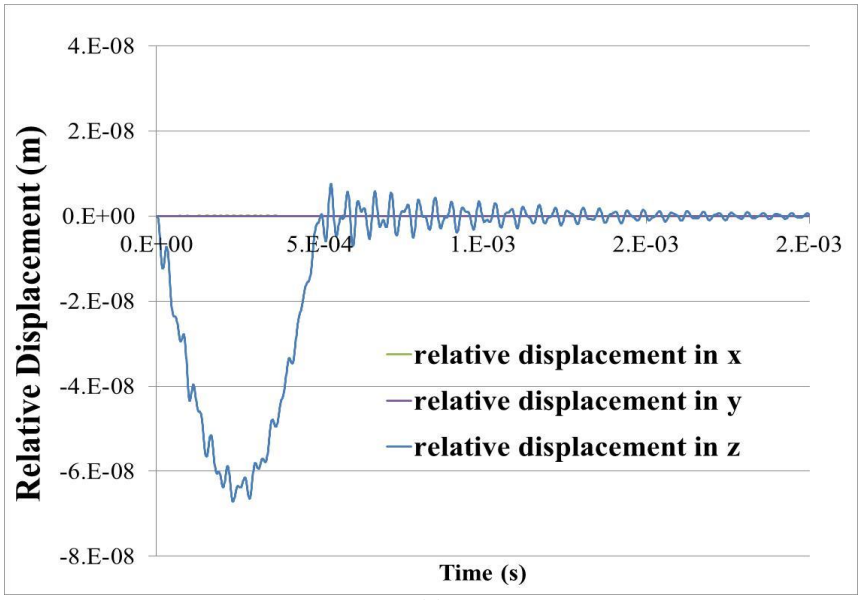

(a)

Fig. 6 Relative displacement of the contact point in *z* direction: (a) the whole time history data along *x*, *y* and *z* directions; (b) the enlarged figure along *z* axis

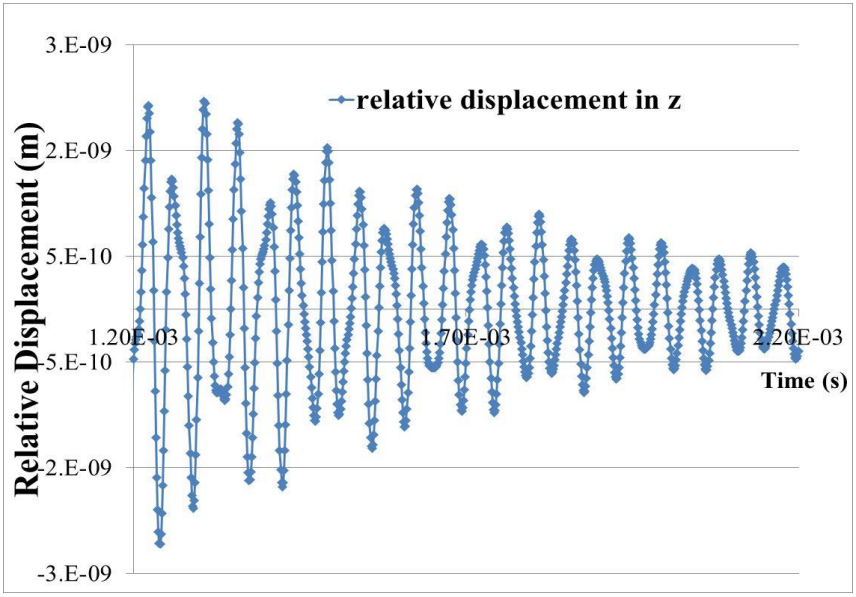

(b)

Fig. 6 Continued

In Fig. 7(a) comparison is made to show the influence of the shock pulse width on the relative displacement of the contact point. It can be seen that during the pulse width, longer pulse results in smoother response curve with a clearer shape of half-sine wave. It can also be observed that higher vibration modes are easier to be excited for shorter pulse width. This is understandable as shorter pulse corresponds to harder contact surface. After the pulse width, the motor oscillations decay faster when the pulse width is longer. As for the maximum magnitude of the relative displacement, they are similar for the three cases. The relative displacement reaches maximum at a time near its input acceleration maximum.

Fig. 8 shows the relative acceleration responses of the contact point for the three pulse widths. Two important observations could be found by examination of the data. Firstly, the acceleration magnitude changes significantly as the shock pulse width varies. Shorter pulse corresponds to higher response acceleration as shorter pulse means stiffer contact surface. When the pulse width decreases from 2 ms to 0.5 ms, the acceleration magnitude increases for about 4 times. When the pulse width further decreases from 0.5 ms to 0.125 ms, the magnitude increases for about 4 times again. Secondly, the acceleration oscillations have similar periods of about 38000 Hz. This corresponds to the 6th vibration mode of the motor (Fig. 4(f)). In this mode, the left or the right beam elongates while the other contracts, causing the contact head to move along z axis. This is the dominating mode when the shock is along z axis.

Besides z direction, shock pulse with different widths in Fig. 5 was also applied to the motor along x and y directions respectively. Fig. 9 shows the relative displacement of the contact point along x axis when the motor experiences a shock in x axis. It is found that for the pulse width of 2ms, 0.5 ms and 0.125 ms, during the shock pulse, along x direction, the relative displacement has an envelope of half-sine curve with the same period as the input pulse. The peak amplitude of the relative displacement is similar for the different pulse widths. When the pulse width decreases, the

sine shape becomes less clear and the peak amplitude slightly increases.

Fig. 10 illustrates the acceleration response of the motor under the shock input in *x* axis. Similar phenomenon as in the case with shock applied in *z* axis can be observed. However, here the dominant oscillating frequency is 33179 Hz, which corresponds to the 5th vibration mode (33587 Hz) of the motor. As shown in Fig. 5 (e), in this mode, the upper and lower beams bend synchronously and the right beam elongates or contracts, causing the contact point to move along *x* axis.

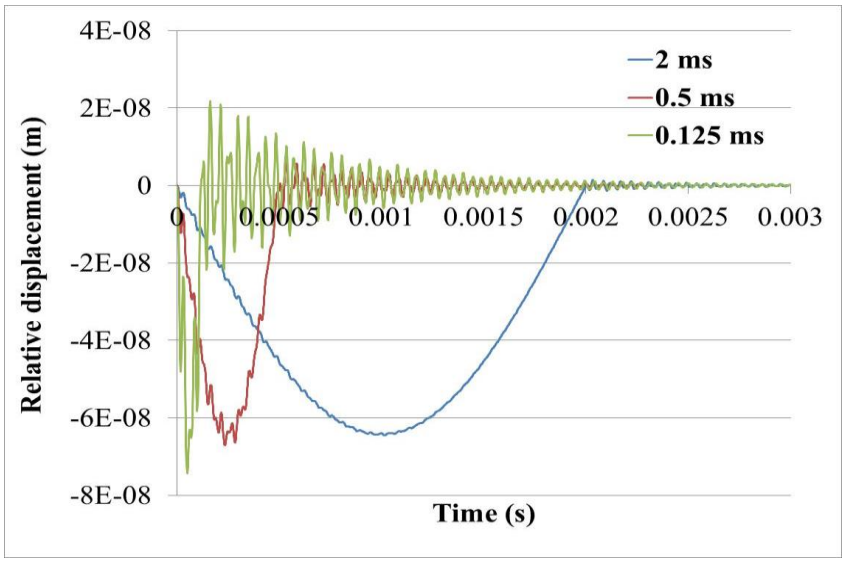

Fig. 7 Time history of the relative displacement for 600 g pulse along *z* axis with different pulse width

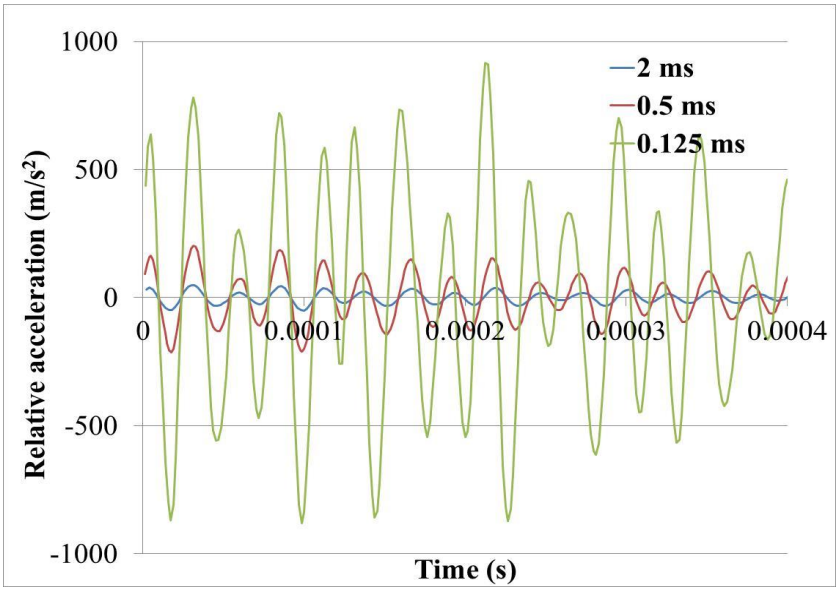

Fig. 8 Acceleration impact responses along z axis for different pulse width

Figs. 11 and 12 show the relative displacement and acceleration of the contact point along *y* axis when the motor experiences a shock in *y* axis. Similarly as for shock in *z* and *x* directions, during the shock width, along *y* direction, the relative displacement has an envelope of a half-sine curve, which has the same period with the input shock pulse. After the shock width, the oscillation periods are the same of 0.114375 ms, which corresponds to 8740.9 Hz. This dominant frequency is also clearly reflected in the acceleration response in Fig. 12. From modal analysis, this frequency corresponds to the 1st vibration mode of the motor with modal frequency of 8740.2 Hz. When the shock is applied along OY direction, this mode is excited and all the three stacks bend along *y* axis, perpendicular to the *xz* plane. This is also the 1st out-of-plane mode of the motor.

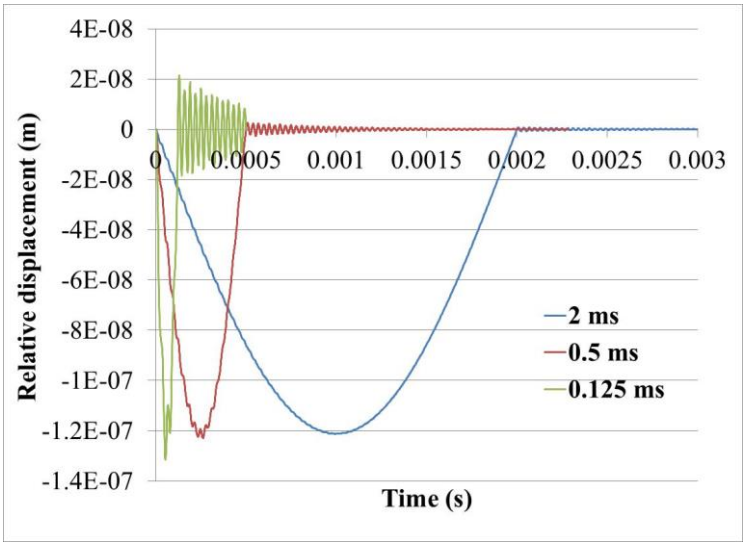

Fig. 9 Time history of the relative displacement for 600 g pulse along *x* axis with different pulse width

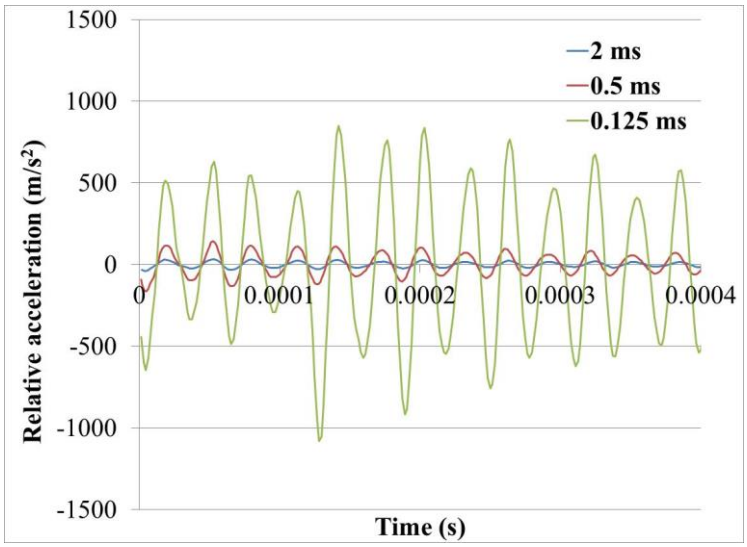

Fig. 10 Acceleration impact responses along *x* axis for different pulse width

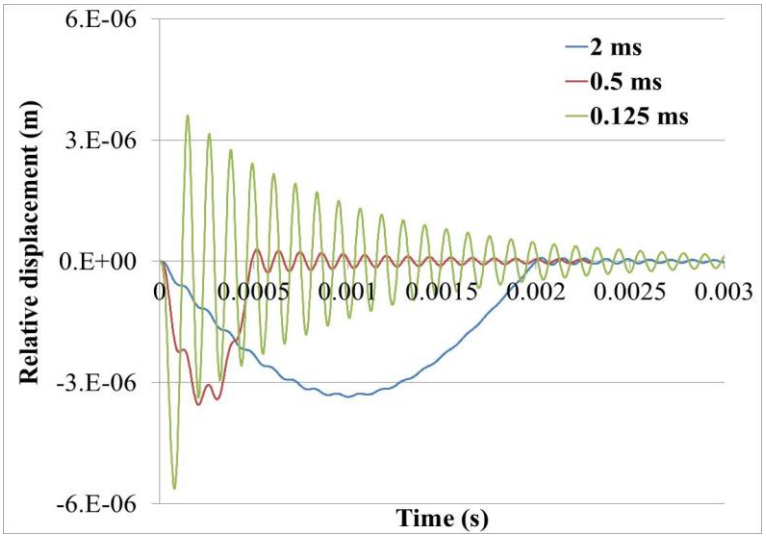

Fig. 11 Time history of the relative displacement for 600 g pulse along *y* axis with different pulse width

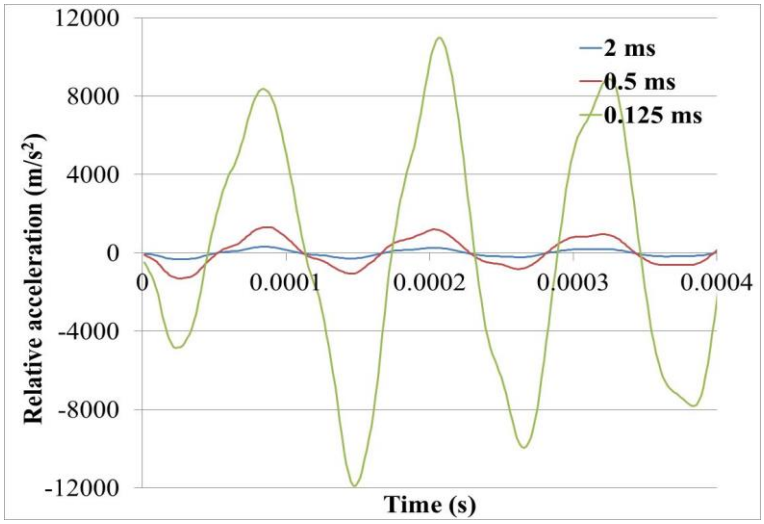

Fig. 12 Acceleration impact responses along *y* axis for different pulse width

After obtaining the motor responses to the shocks in different directions, an examination in the sensitivity of the motor to the shock direction is made. According to Figs. 7, 9 and 11, for a same pulse width say 0.5 ms, the maximum amplitude of the relative displacement is 1.2×10^{-7} m, 3.5×10^{-6} m and 6.6×10^{-8} m for shocks applied in *x*, *y* and *z* directions. Thus we conclude that in the model, the motor under linear drop test is more vulnerable in *y* direction. Investigations in the displacement with other pulse widths and the acceleration data reveal the same phenomenon. However, even along *y* axis, the maximum magnitude of the displacement is of micro meter level which is very small and will not cause damage of the motor or the rotor. This means that the motor is robust enough.

For a shock test, the maximum stress is also desirable to check whether it exceeds the cohesive

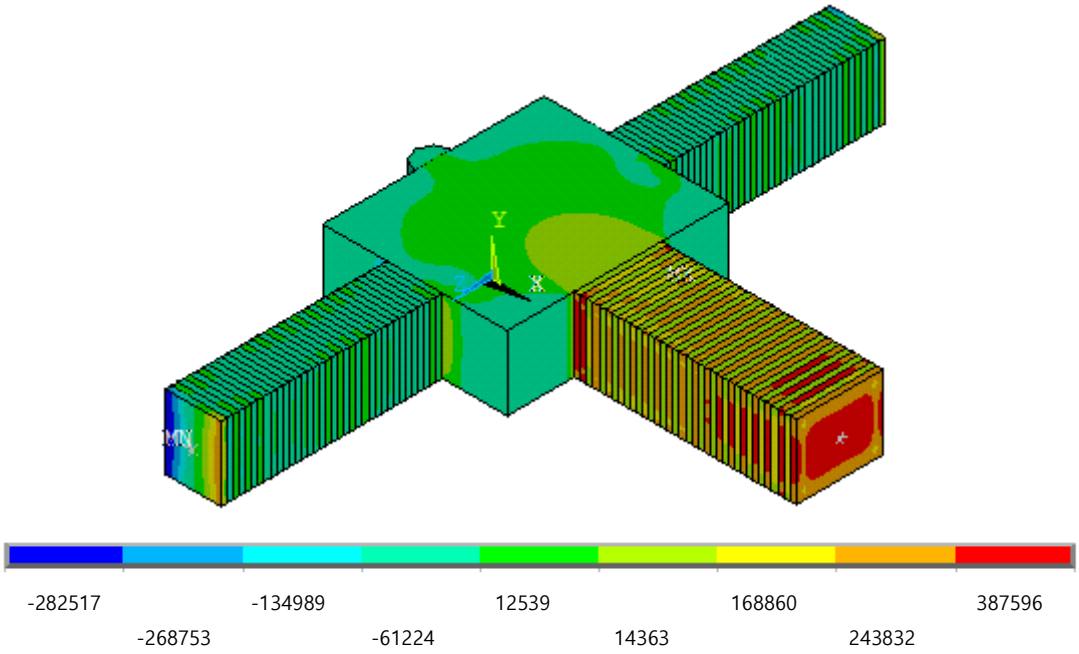

Fig. 13 Stress contours (with color bars in units of N/m^2) of the motor under an acceleration of 600 g along *x* axis with a pulse width of 0.5 ms

strength of the PZT ceramics which will result in fracture of the ceramics. From transient analysis, the maximum stress for each shock case was obtained. Using a shock with 0.5 ms pulse width along *x* axis as an illustration, its maximum stress is 3.88×105 N/m^2 occurring at 0.235 ms as shown in Fig. 13. It is far below the pressure of 2.5×108 N/m^2 under which PZT materials can withstand without breaking. So it is safe to say that for such a shock, the PZT stacks will not break or cause failure.

4. Conclusions

This paper examined the dynamic characteristics of a recently designed ultrasonic motor under shock impulse. In order to do this, half-sine acceleration pulse was applied to the motor and the relative displacement of the mechanical output point of the motor was numerically measured. The effect of the half-sine acceleration pulse was also numerically investigated. It is found that the maximum magnitude of the movement is of micrometer scale. This means that normal impacts will not cause failure of the motor and the new motor design is safe and robust.

Acknowledgements

The financial support of Agency for Science, Technology and Research (A*STAR) grant (Grant

No. 092 156 0137) is gratefully acknowledged.

Reference

ANSYS Structural Manual (2010), ANSYS, Inc.

Chan, Kwong Wah and Liao, Wei-Hsin (2008), "Shock resistance of a disk-drive assembly using piezoelectric actuators with passive damping", *IEEE Trans. Magnet.*, **44**(4), 1633-1638.

Cheon, Seong-Kyu, Jeong, Seong-Su, Lee, Byeong-Ha, Park, Tae-Gone and Park, Jong-Kyu (2016), "Driving characteristics of a hexadecagon-shaped ultrasonic motor", *J. Korean Phys. Soc.*, **68**(1), 93-96.

Guo, Hui, Yao, Junhua, Li, Xunbo and Li, Huafeng (2012), "Mechanism analysis and output characteristics experiments of an ultrasonic motor with circumferential surface drive", *J. Electroceramics*, **28**(2), 118-122.

Ikeda, Takuro (1990), *Fundamentals of Piezoelectricity*, Oxford; New York: Oxford University Press.

Ilene J Busch-Vishniac (1999), *Electromechanical Sensors and Actuators*, Springer, 170.

Lang Brian, W. (2010), "A new American national standard for shock testing equipment", *Sound Vib.*, 14-15.

Paik, Dong-Soo, Yoo, Kyoung-Ho, Kang, Chong-Yun, Cho, Bong-Hee, Nam, Sahn and Yoon, Seok-Jin (2009), "Multilayer piezoelectric linear ultrasonic motor for camera module", *J. Electroceramics*, **22**(1), 346-351.

Randeraat, J.V. and Setterington, R.E. (1974), *Piezoelectric Ceramics*, Mullard Limited.

Sashida, Toshiiku and Kenjo, Takashi (1993), *An Introduction to Ultrasonic Motors*, Clarendon Press-Oxford, 17-20.

Shu, Dong-Wei, Shi, Bao-Jun, Meng, Hui, Yap, Fook Fah and Jiang, Da-Zhi (2007), "Shock analysis of a head actuator assembly subjected to half-sine acceleration pulses", *Int. J. Impact Eng.*, **34**(2), 253-263.

Uchino, Kenji (1999), *Ferroelectric Devices*, Marcel Dekker, 181.

Vasiljev, P., Borodinas, S., Bareikis, R. and Luchinskis, R. (2008), "The square bar-shaped multi-DOF ultrasonic motor", *J. Electroceramics*, **20**(3), 231-235.

Xiaoyan, Hou, Pueh, Lee Heow, Jin, Ong Chong and Piang, Lim Siak (2012), "Design and finite element analysis of a new stack ultrasonic motor based on in-plane mode", *Smart Mater. Struct.*, **21**(11), article id 115002.

Yang, Xiaohui, Liu, Yingxiang, Chen, Weishan and Liu, Junkao (2016), "Sandwich-type multi-degree-of-freedom ultrasonic motor with hybrid excitation", *IEEE Access*, **4**, 905-913.

Zeng, Q.H. and Bogy, D.B. (2002), "Numerical simulation of shock response of disk-suspension-slider air bearing systems in Hard Disk Drives", *Microsyst. Technol.*, **8**(4-5), 289-296.

Zhao, C.S. (2007), *Ultrasonic motors technologies and application*, Beijing, Science Press.

TK